Ultra-high Q Resonators and Sub-GHz Bandwidth Second Order Filters in an SOI Foundry Platform

Deniz Onural*, Hayk Gevorgyan, Bohan Zhang, Anatol Khilo and Miloš A. Popović†
Department of Electrical and Computer Engineering, Boston University, Boston, MA 02215, USA
*onural@bu.edu, †mpopovic@bu.edu

Abstract: We demonstrate racetrack resonators with record-high quality factors reaching 6.6 million in a standard 220 nm silicon photonics foundry platform, and first/second order filters with passbands as narrow as 200 MHz, and 1-5 dB insertion loss. © 2020 The Authors.

1. Introduction

High quality factor, narrow (sub-GHz) linewidth resonators are in demand by many applications of integrated photonics such as sensing devices including gyros [1], optical frequency combs [2], microwave photonic filters [3-7], and are elemental for digital communication [8]. Photonic filters for radio-frequency (RF) signal processing in the optical domain enable drastic reduction in size and weight relative to coupled-metallic-cavity RF filters, as well as wide and dynamic tunability of the RF carrier frequency. If integrated with other active devices such as modulators and photodiodes in foundry photonic silicon-on-insulator (SOI) processes [3], or electronic-photonic platforms [8], they could enable a new generation of microwave photonic systems-on-chip. However, the required bandwidths for microwave photonic filters are 2 to 3 orders of magnitude narrower than typical channel add-drop filters (e.g. 200 MHz vs. 50 GHz) for wavelength division multiplexing. Such bandwidths require resonators with multi-million Q factors that are difficult to achieve in integrated photonics [9], especially in foundry platforms that must support a suite of photonic devices (and perhaps electronics). The 3 dB bandwidth of a resonator-based filter is limited by the loss mechanisms of the resonator, which define its intrinsic quality factor (Q), and in SOI processes are dominated by scattering due to waveguide roughness and radiation due to bending. Recent work has provided a number of approaches for the design of high Q resonators and filters for microwave photonics [4-7,10], most of which trade off free spectral range (FSR), size, single-mode operation and/or foundry compatibility for quality factor.

We present a racetrack resonator design and implementation that reaches a record high Q of 6.6 million, implemented in the 220 nm thick silicon device layer of the standard AIM Photonics multi-project wafer (MPW) silicon photonics foundry process [11]. It has a compact footprint of 13 μm x 0.8 to 2.8 mm, an FSR of 14.5 GHz, and variations of the design with FSRs of 34.6 GHz and 52.8 GHz which maintain Qs over 5 million. First and second-order coupled-cavity filters based on this resonator design yield low insertion losses (IL) of 1-5 dB at 3 dB bandwidths from 200 MHz to 800 MHz. Previous similar SOI implementations have lower Qs and FSRs, reaching up to 2.7 million at 40 GHz FSR [4], 1.1 million at 25 GHz FSR [5], and 3.6 million at an FSR of 2.1 GHz with an all-multimode version exhibiting Q of 1.3 million at 20 GHz FSR [6, 7]. The performance of our resonator design exceeds all previous results in 220 nm silicon in both Q and FSR (with smaller footprint). The resonator design is parametrized to offer a continuous tradeoff of Q (5 to 6 million) vs. FSR (15 to 55 GHz), to support various system requirements.

2. High-Q Racetrack Resonators

Our resonator design is a racetrack, Fig. 1(a), comprising a wide (multimode) waveguide (operated in the single-mode regime in the fundamental mode), single-mode U bends, and connecting tapers, similar to [6]. Improvements in our

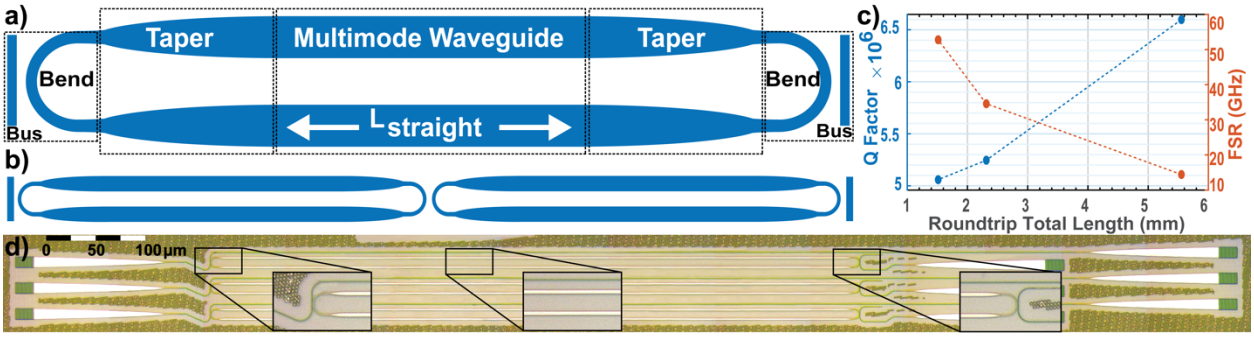

Fig. 1. Racetrack resonator and filter geometry, experimental intrinsic Q vs. FSR trade off and filters optical micrograph. (a) racetrack resonator geometry and building blocks; (b) geometry of a second order filter; (c) intrinsic Q and FSR as a function of the roundtrip total length. (d) Optical micrograph of fabricated first order filters with 52.8 GHz FSR (insets: detail of 2 μm wide waveguide and ring-bus coupling regions). Scale given in the top left; insets are 2.5x magnified relative to the main image.

design include tapered-curvature bends and synthesized compact and efficient tapers that minimize transition losses and increase the achievable Q. And, in our case, the design is implemented in and subject to the design rules of a standard foundry silicon photonics process [11]. The resonators are based on the results of ultra-low silicon waveguide loss of <0.06 dB/cm (due to minimized field overlap with sidewalls of the wide waveguide) and low loss tapers and U bends, recently demonstrated in the same platform for the implementation of a novel, serially connected optical phased array tile, the serpentine optical phased array (SOPA) [12].

The U bends have tapered curvature to minimize radiation and mode-mismatch loss while minimizing path length. A minimum bend length maximizes the Q, since the Q depends on the *average* roundtrip loss. Thus, we want the roundtrip length to be dominated by the ultra-low-loss, wide straight sections. The single mode width of the bends (500 nm) also allows efficient, low-coupler-loss coupling with the 450 nm wide bus waveguides. Compact adiabatic tapers use a synthesized taper shape using the Fourier modal method to minimize length for a given loss [13]. The multimode guide is 2 μm wide with a length, $L_{straight}$ [Fig. 1(a)], varied between 2700 μm and 700 μm to produce different FSRs. Longer lengths produce higher Qs because the taper and bend losses are amortized over a longer ultra-low-loss straight section, and the Q depends on average loss rate. Fabricated resonators had FSRs of 14.5 GHz, 34.6 GHz, and 52.8 GHz, with intrinsic (weakly coupled) quality factors of 6.6, 5.3, and 5 million respectively (shown in Fig. 1(c) vs. the roundtrip total length of the resonator).

3. First Order Filters

First order passband filters provide the narrowest 3 dB bandwidth for a given insertion loss (IL), using a resonator with a given intrinsic Q. Low IL is obtained with equal input and output ring-bus couplings away from critical coupling [14]. Butterworth filters with 3 dB bandwidths of 200 MHz, 400 MHz, and 800 MHz were designed [15].

Experimentally measured responses in Fig. 2(a-c) show the three bandwidths implemented with the different racetrack lengths. An optical micrograph of one set of the fabricated first order filters is shown in Fig. 1(d). All of the filters show bandwidths that are very close to design values. The response with the narrowest bandwidth also has the highest insertion loss, which remains under 1.25 dB, 1.09 dB, and 3.38 dB for the filters with 14.5 GHz, 34.6 GHz, and 52.8 GHz FSR filters, respectively. The resonance of the 200 MHz bandwidth filter with 52.8 GHz FSR showed characteristics of a doublet, likely due to defect induced splitting, which in turn is likely in part responsible for its higher insertion loss. The other line shapes showed single resonance (Lorentzian) characteristics.

4. Vernier Coupled-Resonator Second Order Filters

The spectral performance of bandpass filters (passband flatness and out-of-band rejection) improves with increased filter order (i.e. number of serially coupled resonators) at slight cost in insertion loss [16]. However, the individual cavity resonances must be aligned, which is challenging when the bandwidth is narrow (e.g. 200 MHz), and the sensitivity of each resonance to average waveguide thickness, for example, is ~200 GHz/nm [17]. In this demonstration, we used a Vernier configuration [16] of two rings with slightly differing FSRs to ensure that a passive two-cavity device, without thermo-optic phase shifters, would produce an aligned passband over the wavelength range of interest.

Second order filters were designed by coupling two racetracks with an FSR differential of 0.4 GHz [geometry of Fig. 1(b)], applied by adding a differential length to the second ring that is proportional to the original $L_{straight}$. An effective FSR of the entire two ring system forms as an envelope in the filter spectrum, defined as $1/FSR_{Vernier} = |1/FSR_{V1}-1/FSR_{V2}|$. This effect is illustrated in Fig. 3(a) for the filter with a 14.5 GHz FSR resonator, resulting in an

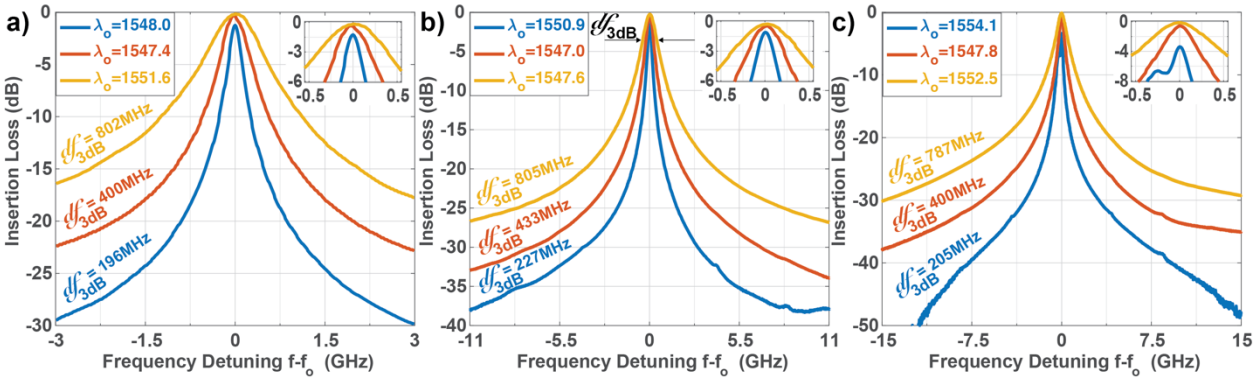

Fig. 2. First order filter responses vs. frequency detuning from center frequency f_o for filters with FSR of 14.5 GHz (a), 34.6 GHz (b), and 52.8 GHz (c). Insertion loss of drop port responses is relative to the out-of-band through port transmission. Top-left insets: center wavelength for each resonance. Top-right insets: zoom-in on resonance peaks. Measured bandwidths of 200 MHz (blue), 400 MHz (red) and 800 MHz (yellow) bandwidth designs written on response curves. Center frequency $f_o=c/\lambda_o$.

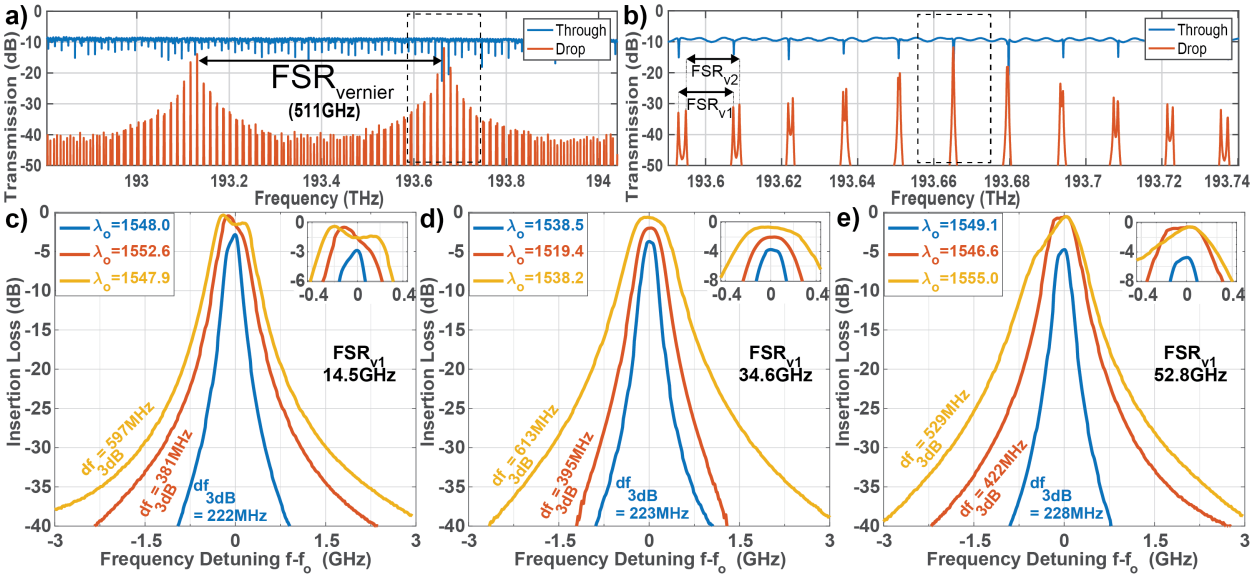

Fig. 3. Second-order filter responses. (a,b): Drop (red) and through (blue) port responses of a 200 MHz passband filter with 14.5 GHz FSR resonators, showing Vernier effect over (a) a wide and (b) narrower range of frequencies. Dotted box in (a) corresponds to region in (b), dotted box in (b) corresponds to the region shown in (c). (c,d,e): Drop port responses vs. frequency detuning from center frequency f_o where the two resonances are aligned, for filters with FSRv1 of 14.5 GHz (c), 34.6 GHz (d), and 52.8 GHz (e). FSRv2 is 0.4 GHz less than FSRv1 for all designs. Drop port insertion loss is relative to through port off-resonance transmission. Top-left insets: center wavelength for each resonance. Top-right insets: zoom-in on resonance peaks. Measured bandwidths of 200 MHz (blue), 400 MHz (red), and 600 MHz (yellow) bandwidth designs written on response curves of the plot. Center frequency $f_o=c/\lambda_o$.

effective FSR of 511 GHz. A close-up is shown in Fig. 3(b), showing how the resonances of 14.5 GHz and 14.1 GHz FSR rings align at one resonant order. FSR_{V1}-FSR_{V2} was set near the bandwidth to ensure at least one passband aligns.

The pass bands of the second order filters are designed for 200 MHz, 400 MHz, and 600 MHz bandwidths. The resulting responses are provided in Fig. 3(c-e), and all passbands showed close to the design specifications. The rolloff is faster than the first order responses, as expected, demonstrating at least 50 dB out of band rejection, and the insertion losses are below 2.85 dB for 14.5 GHz, 3.7 dB for 34.6 GHz, and 4.8 dB for 52.8 GHz FSR filters.

The demonstrated resonators and filters can become a standard component of conventional silicon photonics platforms, and can be utilized alongside modulators, photodiodes and other components for sensing, microwave photonics, and other applications. The current devices were demonstrated in a (Feb 2019) passives fabrication run in the AIM process [11]. Future work remains to evaluate any deleterious effect of the additional processing and thermal cycling steps in an active version of the process. Another step of interest is the implementation of these designs in monolithic electronic-photonic RF-CMOS processes, thereby enabling integration of RF electronics and photonics.

Acknowledgments: This work was funded in part by Ball Aerospace & Technologies Corp. and by the US Government. We would like to thank Todd Pett of Ball Aerospace for valuable input regarding the performance requirements of microwave photonic filters.

5. References

1. B. Wu, Y. Yu, et al., "Silicon integrated interferometric optical gyroscope," Scientific Reports **8,** 8766 (2018).
2. X. Ji, F. A. S. Barbosa, et al., "Ultra-low-loss on-chip resonators with sub-milliwatt parametric oscillation threshold," Optica **4**, 619 (2017).
3. D. Zhou, Y. Yu, et al., "Parallel radio-frequency signal-processing unit based on mode…," Optics Express **26,** 20544-20549 (2018).
4. H. Qiu, F. Zhou, et al., "A continuously tunable sub-gigahertz microwave photonic bandpass…," JLT **36,** 4312-4318 (2018).
5. Y. Zhang, X. Hu, et al., "Design and demonstration of ultra-high-Q silicon microring resonator based on…," Opt. Lett. **43,** 1586-1589 (2018).
6. M. Á Guillén-Torres, K. Murray, et al., "Effects of backscattering in high-Q, large-area…" Opt. Lett. 41, 1538-1541 (2016).
7. M. Burla, B. Crockett, et al., "Ultra-high Q multimode waveguide ring resonators for microwave photonics…," MWP, IEEE, pp. 1-4 (2015).
8. C. Sun, M. Wade, et al., "Single-chip microprocessor that communicates directly using light," Nature **528**, 534 (2015).
9. D. Marpaung, J. Yao, et al., "Integrated microwave photonics," Nature Photonics **13,** 80 (2019).
10. A. Biberman, M. J. Shaw, et al., "Ultralow-loss silicon ring resonators," Opt. Lett. **37**, 4236 (2012).
11. American Institute for Manufacturing (AIM) Photonics: Multi-Project Wafer service, http://www.aimphotonics.com/mpw.
12. B. Zhang, N. Dostart, et al., "Serpentine optical phased array silicon photonic aperture tile…," OFC, OSA, paper M4E.5 (2019).
13. G. H. Song and W. J. Tomlinson, "Fourier analysis and synthesis of adiabatic tapers in integrated optics," JOSA A **9,** 1289-1300 (1992).
14. M. Dašić and M. A. Popović, "Minimum drop-loss design of microphotonic microring-resonator…," TELFOR, paper 6.9, p.927 (2012).
15. A. Melloni and M. Martinelli, "Synthesis of direct-coupled-resonators bandpass filters for WDM systems," JLT **20,** 296 (2002).
16. B. E. Little, S.T. Chu, et al., "Microring resonator channel dropping filters," JLT **15,** 998 (1997).
17. M. A. Popović, T. Barwicz, et al., "Global design rules for silicon microphotonic waveguides…," CLEO, OSA, paper CTuCC1 (2006).